

# Development of High Dielectric Constant Materials Based on Bismuth Copper Titanium Oxide



**Thesis submitted in partial fulfilment**

**For the Award of Degree**

**Doctor of Philosophy**

**By**

**Vishnu Shankar Rai**

**DEPARTMENT OF CHEMISTRY**

**INDIAN INSTITUTE OF TECHNOLOGY**

**(BANARAS HINDU UNIVERSITY)**

**VARANASI-221005**

**Roll No.: 18051507**

**2023**

## CERTIFICATE

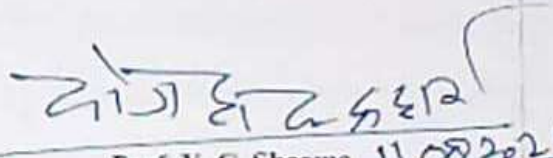
It is certified that the work contained in the thesis entitled "Development of High Dielectric Constant Materials Based on Bismuth Copper Titanium Oxide" by "Mr. Vishnu Shankar Rai" has been carried out under my supervision and this work has not been submitted elsewhere for a degree.

It is further certified that the student has fulfilled all the requirements of Comprehensive examination, Candidacy and SOTA for the award of Ph.D. degree.

  
Prof. K. D. Mandal  
(Supervisor)

Department of Chemistry  
Indian Institute of Technology  
(Banaras Hindu University)  
Varanasi

**Prof. K. D. Mandal**  
Department of Chemistry  
Indian Institute of Technology (IIT) BHU  
Varanasi-221005

  
Prof. Y. C. Sharma 11/08/2023  
(Head)

Department of Chemistry  
Indian Institute of Technology  
(Banaras Hindu University)

Varanasi  
विभागाध्यक्ष / HEAD  
रसायन विज्ञान विभाग  
Department of Chemistry  
भारतीय प्रौद्योगिकी संस्थान (का.हि.वि.वि.)  
Indian Institute of Technology (B.H.U.)  
वाराणसी-221005 / Varanasi-221005

## DECLARATION BY THE CANDIDATE

I, Vishnu Shankar Rai, certify that the work reported in this thesis is my own authentic work and carried out by me under the supervision of Prof. K. D. Mandal from 2019 to 2023, in the Department of Chemistry, Indian Institute of Technology (Banaras Hindu University), Varanasi. The matter embodied in this thesis has not been submitted for the award of any other degree/diploma.

I declare that I have faithfully acknowledged and given credits to the research workers wherever their works have been cited in my work in this thesis. I further declare that I have not fully copied any other's work, paragraphs, text, data, results, etc., reported in journals, books, magazines, reports dissertations, theses, etc., or available at websites and have not included them in this thesis and have not cited as my own work.

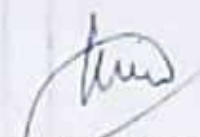
Date: 11/08/2023

Place: IIT (BHU) Varanasi

Vishnu Shankar Rai  
(Vishnu Shankar Rai)

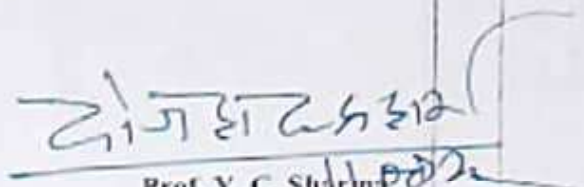
## CERTIFICATE BY THE SUPERVISOR

It is certified that the above statement made by the student is correct to the best of my knowledge.



**Prof. K. D. Mandal**  
(Supervisor)  
Department of Chemistry  
Indian Institute of Technology  
(Banaras Hindu University)  
Varanasi

*Prof. K. D. Mandal*  
Department of Chemistry  
Indian Institute of Technology (IIT),  
Varanasi-221005



**Prof. Y. C. Sharma**  
(Head)  
Department of Chemistry  
Indian Institute of Technology  
(Banaras Hindu University)  
Varanasi

**विभागाध्यक्ष / HEAD**  
रसायन विज्ञान विभाग  
Department of Chemistry  
भारतीय प्रौद्योगिकी संस्थान (का हि वि वि)  
Indian Institute of Technology (B.H.U.)  
वाराणसी-221005 / Varanasi-221005

## COPYRIGHT TRANSFER CERTIFICATE

Title of the Thesis: Development of High Dielectric Constant Materials Based on  
Bismuth Copper Titanium Oxide

Name of the Student: Mr. Vishnu Shankar Rai

### Copyright Transfer

The undersigned hereby assigns to the Indian Institute of Technology (Banaras Hindu University) Varanasi all rights under copyright that may exist in and for the above thesis submitted for the award of the "Doctor of Philosophy".

Date: 11/09/2023

Signature of the Student

Vishnu Shankar Rai

Place: Varanasi

(Vishnu Shankar Rai)

**Note:** However, the author may reproduce or authorize others to reproduce material extracted verbatim from the thesis or derivative of the thesis for the author's personal use provided that the source and the Institute's copyright notice are indicated.



**DEDICATED**

**TO MY**

**PARENTS**

## ACKNOWLEDGMENTS

I would like to express my heartfelt gratitude to my supervisor **Prof. K. D. Mandal**, Department of Chemistry, Indian Institute of Technology, (B.H.U) for allowing me to join his research group, and for providing the precursor base knowledge for my research. Through his unflinching support, constructive criticism, his scientific intuition and advice, he exceptionally inspired me and enriched my growth as a researcher. His involvement nourished my intellectual maturity, provided me opportunities to collaborate with other scientists, that going to help me throughout my career.

My sincere gratitude is also expressed to **Prof. Y. C. Sharma**, Head, and **Prof. D. Tiwary**, Former Head, Department of Chemistry, Indian Institute of Technology, (B.H.U) Varanasi, for his fruitful suggestions and providing research facilities available in the Department.

It is my great pleasure to thanks my RPEC members **Dr. Jeyakumar Kandasamy**, **Prof. D. Tiwary** from Department of Chemistry, Indian Institute of Technology (B.H.U) Varanasi and **Prof. Satya Vir Singh**, Department of Chemical Engineering, Indian Institute of Technology, (B.H.U) for giving valuable suggestions throughout my Ph.D. program.

I also want to acknowledge the In-charge and members of the Central Instrumentation Facility Center (CIFC) and office staff of the Chemistry Department for their help and support.

My special thank goes to my senior and good friend **Dr. Laxman Singh**, **Dr. Shiva Sundar Yadava**, **Dr. Atendra Kumar**, **Dr. Vinod Kumar**, **Dr. Manish Kumar Verma**, **Dr. Shruti Singh**, **Dr. Santosh Pandey** from Department of Chemistry Indian Institute of Technology, (B.H.U), and **Dr. Tapas Das**, **Dr. Ravi Kumar Sonawani**, and **Dr. Kedar Sahoo** from Department of Chemical Engineering, Indian Institute of Technology, (B.H.U) for useful discussions and help throughout my research.

## ACKNOWLEDGMENTS

I would also like to thank to my lab mates **Mr. Alok Kumar Singh, Mr. Dinesh Prajapati, Mr. Anup Kumar,** and **Mr. Biswajit Jena** for their active support.

I am very much thankful to all faculty members of the Department for their encouragement and support.

I heartily thank my best friends **Ms. Priyanka Maurya, Mr. Ved Vyas, Mr. Abhimanyu Yadav, Mr. Vivek Kumar, Mr. Sarvatej Kumar Maurya,** and **Ms. Shraddha Jaiswal** for encouraging me to get enrolled for this degree.

Parents are God on earth and I am very lucky to have very caring and loving parents **Shri Ashok Kumar Rai** and **Smt. Sheela Rai**. I would like to put in words my gratitude to my family members **Smt. Chandravati Devi, Mr. Vinod Rai, Mr. Ravi Shankar Rai, Mr. Rakesh Rai, Mr. Sandeep Kumar Rai,** and **Mr. Akash Rai,** and special thanks to my siblings **Mrs. Suman Rai, Mrs. Pooja Rai, Mrs. Archana Rai, Mrs. Shweta Rai and Sonal Rai** for making my life happy with their constant love and moral supports.

I wish to express my special thanks to DST, Government of India for providing financial support as INSPIRE fellowship to carry out this work.

Last but not least, I thank **Almighty God** for providing me strength and courage to do this work.

Date:

Place: Varanasi

(Vishnu Shankar Rai)

## *Contents*

<b>Contents</b>		<b>Page No.</b>
<b>Title of Thesis</b>		<b>i</b>
<b>Certificate</b>		<b>ii</b>
<b>Declaration by the Candidate &amp; Certificate by the Supervisor</b>		<b>iii-iv</b>
<b>Copyright Transfer Certificate</b>		<b>v</b>
<b>Dedication</b>		<b>vi</b>
<b>Acknowledgements</b>		<b>vii-viii</b>
<b>Contents</b>		<b>ix-xii</b>
<b>List of Figures</b>		<b>xiii-xviii</b>
<b>List of Tables</b>		<b>xix</b>
<b>List of symbols/ Abbreviation</b>		<b>xx-xxi</b>
<b>Preface</b>		<b>xxii-xxviii</b>
<b>CHAPTER – 1 Introduction</b>		<b>1-65</b>
1.1 Materials science		1
1.2 Classifications of nanostructured materials		2
1.3 Metal oxides and mixed metal oxides nanoparticles		4
1.4 Applications of metal oxides and mixed metal oxides nanoparticles		8
1.5 Perovskite oxides: A General Introduction		12
1.6 Classification of Perovskite		18
1.7 Type and Structures of Perovskite		18-24
(a)	ABO <sub>3</sub> Perovskite	18
(b)	A <sup>+1</sup> B <sup>+5</sup> O <sub>3</sub> Perovskite	19
(c)	A <sup>+2</sup> B <sup>+4</sup> O <sub>3</sub> Perovskite	20
(d)	A <sup>+3</sup> B <sup>+3</sup> O <sub>3</sub> Perovskite	20
(e)	(ABO <sub>3</sub> ) <sub>n</sub> AO Perovskite	21
(f)	A <sub>2</sub> B <sub>2</sub> O <sub>5</sub> Perovskite	21
1.8 Complex perovskites		25
1.9 Substitutions in perovskite		26
1.10 Chemical synthesis routes for ceramic material		29
1.11 Dielectric properties of metal oxide		31-35
1.11.1	Capacitors	31
1.11.2	Dielectric materials	33

## *Contents*

1.12 Electrical Polarization		35-38
1.12.1	Orientation Polarization	35
1.12.2	Space Charge Polarization	36
1.12.3	Atomic or Ionic Polarization	36
1.13 Dielectric constant		38
1.14 Dielectric loss		39
1.15 Impedance		40
1.16 Electrical conductivity		43
1.17 Aim of study		44
References		47
<b>CHAPTER–2 Materials Synthesis and Characterizations</b>		<b>66-76</b>
2.1 Experimental procedure		66
2.2 Synthesis of materials		67-68
(a)	Semi wet route	67
(b)	Preparation of ceramic material	67
2.3 Calcination process		69
2.4 Sintering process		69
2.5 X-Ray Diffraction analysis		69
2.6 Transmission Electron Microscopy (TEM) analysis		71
2.7 Scanning Electron Microscopy (SEM) analysis		72
2.8 Energy Dispersive X-ray analysis (EDX)		73
2.9 Electric and Dielectric measurement		74
2.10 Electrochemical characterization		76
<b>CHAPTER – 3 Investigation of microstructure and dielectric behavior of <math>\text{Bi}_{2/3}\text{Cu}_{3-x}\text{Mg}_x\text{Ti}_4\text{O}_{12}</math> (<math>x=0, 0.05, 0.1</math> and <math>0.2</math>) ceramics synthesized by semi-wet route</b>		<b>77-99</b>
3.1 Introduction		77
3.2 Material synthesis and characterization		79
3.3 Results and discussion		80-92
3.3.1	X-Ray diffraction (XRD) analysis	80
3.3.2	Scanning Electron Microscopy (SEM) analysis	81
3.3.3	Transmission Electron Microscopy (TEM) analysis	82
3.3.4	X-ray photoelectron spectroscopic (XPS) studies	83

## *Contents*

3.3.5	Dielectric studies	86
3.3.6	Impedance spectroscopic studies	88
3.3.7	Conductivity measurements	90
3.4	Conclusions	92
	References	93
<b>CHAPTER –4 Low temperature Synthesis, dielectric and electrical characteristics of <math>\text{Bi}_{2/3}\text{Cu}_{3-x}\text{Ni}_x\text{Ti}_4\text{O}_{12}</math> (where <math>x=0.05, 0.1, \text{ and } 0.2</math>) ceramics</b>		<b>100-123</b>
4.1	Introduction	100
4.2	Material synthesis and characterization	102
4.3	Results and discussion	104-118
4.3.1	X-Ray diffraction (XRD) analysis	104
4.3.2	Microstructural studies	106-109
4.3.2.1	Scanning Electron Microscopy (SEM) Studies	106
4.3.2.2	Transmission Electron Microscopy (TEM) Studies	108
4.3.3	X-Ray Photoelectron Spectroscopic (XPS) Studies	109
4.3.4	Dielectric studies	111
4.3.5	Conductivity measurement	112
4.3.6	Electrochemical studies	114
4.4	Conclusions	117
	References	119
<b>CHAPTER – 5 Influence of Zn doping on microstructure, dielectric and electrical properties in <math>\text{Bi}_{2/3}\text{Cu}_3\text{Ti}_4\text{O}_{12}</math> ceramic synthesized by the semi wet method</b>		<b>124-152</b>
5.1	Introduction	124
5.2	Materials synthesis and characterizations	125
5.3	Results and discussion	127-144
5.3.1	X-Ray diffraction (XRD) analysis	127
5.3.2	Microstructural studies	128-133
5.3.2.1	Scanning Electron Microscopic (SEM) studies	128
5.3.2.2	Transmission Electron Microscopic (TEM) studies	131
5.3.3	X-Ray Photoelectron Spectroscopic (XPS) studies	133
5.3.4	Dielectric studies	135
5.3.5	Impedance spectroscopic studies	137

## *Contents*

---

5.3.6	Electrical conductivity	140
5.3.7	Cyclic Voltammetry	143
5.4 Conclusions		144
References		145
<b>CHAPTER – 6 Emergence of dielectric properties by doping of semi-transition metal in semi-conductor complex perovskite oxide</b>		<b>153-177</b>
6.1 Introduction		153
6.2 Materials synthesis and characterization		155
6.3. Results and discussion		157-172
6.3.1	X-ray Diffraction (XRD)	157
6.3.2	Scanning Electron Microscopic (SEM) studies	158
6.3.3	Transmission Electron Microscopic (TEM) studies	160
6.3.4	X-Ray Photoelectron Spectroscopic (XPS) studies	162
6.3.5	Dielectric studies	164
6.3.6	Impedance spectroscopic studies	167
6.3.7	Electrical conductivity	168
6.3.8	Cyclic Voltammetry	170
6.4 Conclusions		172
References		173
<b>CHAPTER – 7 Summary and Future Scope</b>		<b>178-179</b>
7.1 Summary		178
7.2 Future scope		179
<b>List of Publications</b>		<b>180-182</b>

## ***LIST OF FIGURES***

---

	<b>Page No.</b>
Fig. 1.1. Schematic presentation of reduced-dimensional systems.	3
Fig. 1.2. SEM image of the Ce <sub>2</sub> O <sub>3</sub> –TiO <sub>2</sub> composite nanofibers.	6
Fig. 1.3.. SEM image of ZnO nanorings.	6
Fig. 1.4. SEM image of NiO nanotubes.	7
Fig. 1.5. SEM image of flower-like CuO.	7
Fig. 1.6. TEM image of $\gamma$ -Fe <sub>2</sub> O <sub>3</sub> spherical nanoparticles.	8
Fig. 1.7. Application of metal oxides and mixed metal oxides nanoparticles in various fields.	11
Fig. 1.8. Classification of perovskite.	18
Fig. 1.9. The structure of ABO <sub>3</sub> perovskite.	19
Fig. 1.10. Structure of Ca <sub>2</sub> Mn <sub>2</sub> O <sub>5</sub> unit cell showing oxygen vacancy along the direction of normal A B plane.	22
Fig. 1.11. . Crystal structure of Bi <sub>2/3</sub> Cu <sub>3</sub> Ti <sub>4</sub> O <sub>12</sub> (BCTO).	26
Fig.1.12. Shows parallel plate capacitors in circuit, including the alignment of charges in the dielectric material.	32
Fig.1.13. The polarized and non-polarized plates of an applied electric field.	33
Fig. 2.1. Flow chart for the synthesis of complex perovskite by the semi-wet route.	71
Fig. 2.2. Powder X-ray diffractometer, RigakuMiniflex600 (Japan).	70
Fig. 2.3. Transmission Electron Microscope (TEM, FEI TECANI G <sup>2</sup> 20 TWIN, USA) used to determining particle structure	72

- Fig. 2.4. Scanning Electron Microscope (ZEISS, model EVO-18 Research) used for microstructure of the surface of the ceramics 73
- Fig. 2.5. LCR Meter (PSM 1735, Newton 4th Ltd, U.K.) used for dielectric properties measurement 75
- Fig. 3.1. XRD Pattern of BCTO, BCMgTO-0.05, BCMgTO-0.1, and BCMgTO-0.2 ceramics sintered at 1173 K for 8 h. 81
- Fig. 3.2. SEM images of (a) BCTO (b) BCMgTO-0.05 (c) BCMgTO-0.1 and (d) BCMgTO-0.2 ceramics 82
- Fig. 3.3. Bright-field TEM image; b SAED pattern of BCMgTO-0.2 ceramic sintered at 1173 K for 8 h. 83
- Fig. 3.4. XPS spectra of (a) Cu (b) Bi, (c) Mg; (d) Ti; (e) O of BCMgTO-0.2 ceramic sintered at 1173 K for 8 h. 85
- Fig. 3.5. Frequency dependence of (a) dielectric constant( $\epsilon_r$ ); (b) dielectric loss ( $\tan \delta$ ) for BCTO, BCMgTO-0.05, BCMgTO-0.1, and BCMgTO-0.2 ceramics sintered at 1173 K for 8 h. 86
- Fig. 3.6. Temperature dependence of (a) dielectric constant( $\epsilon_r$ ); (b) tangent loss ( $\tan \delta$ ) of BCTO, BCMgTO-0.05, BCMgTO-0.1; BCMgTO-0.2 ceramics sintered at 1173 K for 8 h. 87
- Fig. 3.7. (a) Complex impedance plot or cole-cole plot ( $Z''$  vs  $Z'$ ), (b) frequency dependence of imaginary part of impedance ( $Z''$ ) and (c) frequency dependence of real part of impedance ( $Z'$ ) at 303 K for BCTO, BCMgTO-0.05, BCMgTO-0.1 and BCMgTO-0.2 ceramics. 89

- Fig. 3.8. (a) Plots of conductivity ( $\ln \sigma$ ) with the inverse of temperature at 10 kHz; (b) frequency dependence of AC conductivity at 303K for BCTO, BCMgTO-0.05, BCMgTO-0.1 and BCMgTO-0.2 ceramics. 90
- Fig. 4.1. XRD Pattern of BCNTO-0.05, BCNTO-0.1, and BCNTO-0.2 ceramics sintered at 1123 K for 8 h. 105
- Fig. 4.2. SEM images of a BCNTO-0.05; b BCNTO-0.1; cBCNTO-0.2 ceramics sintered at 1123 K for 8 h. 107
- Fig. 4.3. EDX spectra of a BCNTO-0.05; b BCNTO-0.1; c BCNTO-0.2 ceramics sintered at 1123 K for 8 h. 108
- Fig. 4.4. a-c TEM images and (d-f) SAED pattern of BCNTO-0.05, BCNTO-0.1, and BCNTO-0.2 ceramics sintered at 1123 K for 8 h respectively. 109
- Fig. 4.5. XPS spectra of a Bi; b Cu; c Ni; d Ti;e O of BCNTO-0.2 ceramic sintered at 1123 K for 8 h. 110
- Fig. 4.6. Frequency dependence of a dielectric constant( $\epsilon_r$ ) at 470 K; b dielectric loss ( $\tan \delta$ ) for BCNTO-0.05, BCNTO-0.1, and BCNTO-0.2 ceramics at 310 K. 111
- Fig. 4.7. Temperature dependence of a dielectric constant( $\epsilon_r$ ); b tangent loss ( $\tan \delta$ ) of BCNTO-0.05, BCNTO-0.1 and BCNTO-0.2 ceramics at 10 kHz. 112
- Fig. 4.8. a Plots of Conductivity ( $\ln \sigma$ ) with the inverse of temperature at 10 kHz; b frequency dependence of AC conductivity at 310 K for BCNTO-0.05, BCNTO-0.1, and BCNTO-0.2 ceramics. 113
- Fig. 4.9. Cyclic Voltammetry plot of BCNTO-0.05, BCNTO-0.1, and 115

---

BCNTO-0.2 ceramics sintered at 1123 K for 8 h.

Fig. 4.10. Frequency dependence of real part of impedance of BCNTO- 116  
0.05, BCNTO-0.1, and BCNTO-0.2 ceramics.

Fig. 4.11. Nyquist plot of BCNTO-0.05, BCNTO-0.1, and BCNTO-0.2 117  
ceramics.

Fig. 5.1. XRD Pattern of BCTO, BCZTO-0.05, BCZTO-0.1 and 128  
BCZTO-0.2 ceramics sintered at 1123 K for 8 h.

Fig. 5.2. SEM images of a BCTO; b BCZTO-0.05; c BCZTO-0.1; d 129  
BCZTO-0.2 ceramics.

Fig. 5.3. EDX images of a BCTO; b BCZTO-0.05; c BCZTO-0.1; d 130  
BCZTO-0.2 ceramics.

Fig. 5.4. a and b Bright-field TEM images; c and d SAED pattern of 132  
BCZTO-0.05, BCZTO-0.1ceramics respectively.

Fig. 5.5. a Bright-field TEM image; b SAED pattern of BCZTO-0.2 133  
ceramic.

Fig. 5.6. XPS spectra of a Bi;b Cu; c O; d Ti; e Zn of BCZTO-0.2 134  
ceramic.

Fig. 5.7. Variation of a dielectric constant ( $\epsilon_r$ ) and b tangent loss ( $\tan \delta$ ) 135  
with frequency at 310 K for BCTO, BCZTO-0.05, BCZTO-0.1, and  
BCZTO-0.2 ceramics.

Fig. 5.8. Variation of a dielectric constant( $\epsilon_r$ ) and b tangent loss ( $\tan \delta$ ) 136

with temperature at 10 kHz for BCTO, BCZTO-0.05, BCZTO-0.1, and BCZTO-0.2 ceramics.

Fig. 5.9. Complex impedance plot or Nyquist plot ( $Z''$  vs  $Z'$ ) at 350 K for a BCTO; b BCZTO-0.05; c BCZTO-0.1; d BCZTO-0.2 ceramics. 137

Fig. 5.10. Frequency dependence of imaginary part of impedance ( $Z''$ ) at selected temperatures for a BCTO; b BCZTO-0.05; c BCZTO-0.1; d BCZTO-0.2 ceramics. 139

Fig. 5.11. Plots of conductivity ( $\ln \sigma$ ) with the inverse of temperature at selected frequencies for a BCTO; b BCZTO-0.05; c BCZTO-0.1; d BCZTO-0.2 ceramics. 140

Fig. 5.12. Frequency dependence of AC conductivity ( $\ln \sigma_{ac}$ ) at selected temperatures for a BCTO; b BCZTO-0.05; c BCZTO-0.1; d BCZTO-0.2 ceramics. 141

Fig. 5.13. Cyclic Voltammetry plots for a BCTO; b BCZTO-0.05; c BCZTO-0.1; d BCZTO-0.2 ceramics. 144

**Fig. 6.1.** XRD Pattern of BCTGO-0.05 and BCZTGO-0.05 ceramics sintered at 1123 K for 8 h. 158

**Fig. 6.2.** SEM images of (a) BCTGO-0.05 and (b) BCZTGO-0.05 ceramics sintered at 1123 K for 8 h. 159

**Fig. 6.3.** EDX images (a) BCTGO-0.05 and (b) BCZTGO-0.05 ceramics sintered at 1123 K for 8 h. 159

**Fig. 6.4.** (a), (b) TEM images and (c), (d) SAED pattern of BCTGO-0.05 and BCZTGO-0.05 ceramics sintered at 1123 K 161

for 8 h respectively.

**Fig. 6.5.** XPS spectra of (a) Bi, (b) Cu, (c) Ti, (d) Ge, and (e) O of BCTGO-0.05 ceramic sintered at 1123 K for 8 h. 162

**Fig. 6.6.** XPS spectra of (a) Bi, (b) Cu, (c) Zn, (d) Ti, (e) Ge, and (f) O of BCZTGO-0.05 ceramic sintered at 1123 K for 8 h. 163

**Fig. 6.7.** Frequency dependence of dielectric constant( $\epsilon_r$ ) of (a) BCTGO-0.05 and (b) BCZTGO-0.05; Frequency dependence of dielectric loss ( $\tan \delta$ ) for (c) BCTGO-0.05 and (d) BCZTGO-0.05 ceramics at few selected temperatures. 165

**Fig. 6.8.** Temperature dependence of dielectric constant ( $\epsilon_r$ ) of (a) BCTGO-0.05 and (b) BCZTGO-0.05; Frequency dependence of dielectric loss ( $\tan \delta$ ) for (c) BCTGO-0.05 and (d) BCZTGO-0.05 ceramics at few selected frequencies. 166

**Fig. 6.9.** frequency dependence of imaginary part of impedance ( $Z''$ ) of (a) BCTGO-0.05 and (b) BCZTGO-0.05; Complex impedance plot ( $Z''$  vs  $Z'$ ) of (c) BCTGO-0.05 and (d) BCZTGO-0.05 ceramics at few selected temperatures. 167

**Fig. 6.10** Plots of Conductivity ( $\ln \sigma$ ) with the inverse of the temperature of (a) BCTGO-0.05 and (b) BCZTGO-0.05; frequency dependence of AC conductivity of (c) BCTGO-0.05 and (d) BCZTGO-0.05 ceramics 169

**Fig. 6.11**(a) Cyclic voltammetry, (b) Nyquist plot, (c) Frequency vs total impedance plot, (d) Frequency vs net capacitance plot of BCZTGO-0.05 and BCTGO-0.05 ceramics. 171

## *LIST OF TABLES*

---

	<b>Page No.</b>
Table 1.1 Example of some perovskite explaining Typical property application and their use.	23-24
Table 1.2 Shows polarization mechanism of dielectric materials.	37-38
Table 1.3 High dielectric constant of few oxide compounds.	42-43
Table 2.1 Specification of the materials used for Synthesis.	66-67
Table 5.1 The data of grain and grain boundary resistance for Zn-doped and undoped BCTO	138-139
Table 5.2 The value of power law exponent (s) for BCTO, BCZTO-0.05, BCZTO-0.1, and BCZTO-0.2 ceramics at few selected temperatures.	142

## LIST OF SYMBOLS/ ABBREVIATIONS

---

$t$	Tolerance factor
$E$	Electric field
$\epsilon_0$	Permittivity of free space
$P$	Electrical dipole moment
$\chi_e$	Dielectric susceptibility
$n$	Unitless constant
$\epsilon_r$	Relative permittivity
$E_{loc}$	Local field
$P_{mol}$	Moment
$\alpha'$	Polarizability
$N$	Molecules per unit volume
$k$	Relative dielectric constant
$\epsilon^*$	Complex Quantity of dielectric constant
$\epsilon'$	Real components of dielectric constant
$\epsilon''$	Imaginary component of dielectric constant
$i$	Imaginary number
$D_f$	Dissipation factor
$\tan \delta$	Tangent loss
$W$	Energy loss
$\epsilon_r$	Relative dielectric constant
$C$	Capacitance
$F$	Farad

## LIST OF SYMBOLS/ ABBREVIATIONS

---

$\sigma$	Conductivity
f	Frequency
$P_{\text{electronic}}$	Electronic polarization
$P_{\text{ionic}}$	Ionic polarization
$P_{\text{molecular}}$	Molecular polarization
$P_{\text{interfacial}}$	Interfacial polarization
Hz	Hertz
$\lambda$	Wavelength
$\theta$	Angle theta
$^{\circ}\text{C}$	Degree centigrade
K	Kelvin
$k_{\text{B}}$	Boltzmann constant
P	Net polarization
$\omega$	Angular frequency
$\tau$	Relaxation time
Å	Angstrom
R	Resistance
C	Capacitance
$Z'$	Real impedance
$Z''$	Imaginary impedance
$M'$	Real modulus
$M''$	Imaginary modulus

Perovskite oxides, known for their high dielectric constant, have found significant applications due to this property. Their general formula is  $ABO_3$ , where A represents an alkaline earth ion, and B denotes a transition metal ion. These compounds have been extensively studied because of their intriguing properties in the realms of dielectric, electrical, piezoelectric, and optoelectronic phenomena.

Perovskites can be modified through various substitutions on either the A-site or the B-site, resulting in structures like  $AA'BO_3$  and  $ABB'O_3$ . These substitutions may involve isovalent or heterovalent elements. Ferroelectric materials typically exhibit dielectric constants higher than 1,000. However, the dielectric constant demonstrates a peak concerning temperature. The undesirable temperature dependence of the dielectric constant near the peak temperature poses challenges for certain applications. The specific site occupied by an element in the parent compound, as well as the composition range for solid solution formation, depends on parameters such as radius, valency, and coordination number.

We have reported here the results of our investigation on a class of compounds having perovskite related structure. These have dielectric properties very different from those of ferroelectrics or relaxors. Their high dielectric constant shows only a small dependence on temperature.

The  $ACu_3Ti_4O_{12}$  family of compounds has been known since 1967, and in 1979, its family was expanded, and more accurate structures were determined. However, it was not until after the year 2000 that the dielectric properties of these compounds were thoroughly studied. Among the oxides in this family,  $ACu_3Ti_4O_{12}$  types exhibit

## PREFACE

---

remarkably high dielectric constants. Particularly,  $\text{CaCu}_3\text{Ti}_4\text{O}_{12}$  stands out with a dielectric constant of about 12,000 at 1 kHz and a low loss tangent ( $\sim 10^{-1}$ ), maintaining this behavior in the temperature range of 100-600 K and across frequencies from  $10^2$  to  $10^6$  Hz. This exceptional property makes it an ideal thermally stable material with a high dielectric constant. The cubic structure of these compounds is related to that of perovskite, specifically  $\text{CaTiO}_3$ , further supporting their suitability as high dielectric constant materials. However, below 100 K, the dielectric constant value drops dramatically to around 100. Notably, neutron powder diffraction studies indicate no change in the crystal structure within the temperature range of 298-1273 K.

Structure of  $\text{CaCu}_3\text{Ti}_4\text{O}_{12}$  is much more constrained than the usual perovskite structure.  $\text{TiO}_6$  octahedra have tilted to form a square planar arrangement around  $\text{Cu}^{2+}$ . If one assumes that both Ti-O and Cu-O distances are  $1.96 \text{ \AA}$  and that the Ti-O octahedron is not distorted, one finds that the unit cell edge must be  $7.383 \text{ \AA}$  and the Ca-O distance should be  $2.61 \text{ \AA}$ . A small deviation of the O-Ti-O angles from  $90^\circ$  produces the experimentally determined values of  $a = 7.391 \text{ \AA}$  and  $\text{Ca-O} = 2.604 \text{ \AA}$ . This Ca-O distance is much less than the  $2.72 \text{ \AA}$ , a value predicted based on the ionic radii. The situation is then similar to that in  $\text{BaTiO}_3$ , where the Ba-O distance of  $2.84 \text{ \AA}$  is much less than the predicted value of  $2.99 \text{ \AA}$ , on the basis of sum of ionic radii. Thus, in both  $\text{BaTiO}_3$  and  $\text{CaCu}_3\text{Ti}_3\text{O}_{12}$ , the  $\text{A}^{2+}$  cation is in a site too small for it. As it pushes out to expand the lattice, it places the Ti-O bonds under tension and increases the polarizability of the  $\text{TiO}_6$  octahedra.

In the cubic perovskite structure encountered in  $\text{BaTiO}_3$  above 393 K, the  $\text{Ti}^{4+}$  cation is in a site of full cubic symmetry. With decreasing temperature,  $\text{Ti}^{4+}$  displaces toward one,

## PREFACE

---

then two and finally three oxygen anions, to produce, respectively, the tetragonal, orthorhombic, and rhombohedral ferroelectric structures. The site symmetry for  $\text{Ti}^{4+}$  in  $\text{CaCu}_3\text{Ti}_4\text{O}_{12}$  is much lower than that in cubic  $\text{BaTiO}_3$ ; this greatly reduces the possibility of a ferroelectric phase transition based on the displacement of  $\text{Ti}^{4+}$  from the center of its octahedron. For example, the lack of a fourfold axis in the  $\text{Im}3$  space group for  $\text{CaCu}_3\text{Ti}_4\text{O}_{12}$  eliminates the possibility of a transition to a tetragonal ferroelectric structure. The  $\text{Ti}^{4+}$  cations could displace off center along their one threefold axis. However, this could not be a pure ferroelectric transition because the displacements would actually occur along four different directions. Thus, we have in  $\text{CaCu}_3\text{Ti}_4\text{O}_{12}$ , a perovskite-type structure, where polarizability and dielectric constant are enhanced by tension on the Ti-O bonds, but where a transition to a ferroelectric state is frustrated by the  $\text{TiO}_6$  octahedra tilt structure that accommodates the square planar coordination of  $\text{Cu}^{2+}$ . Substitution of  $\text{Zn}^{2+}$ ,  $\text{Mg}^{2+}$  and  $\text{Ni}^{2+}$  at  $\text{Cu}^{2+}$  site and  $\text{Ge}^{4+}$  at Ti site gives rise to interesting useful properties. Therefore it was considered worthwhile to investigate the effect of their independent substitution as well as simultaneous substitution in equimolar concentration at  $\text{Cu}^{2+}$  and  $\text{Ti}^{4+}$  sites. We have also studied the Nickel and Germanium doping at copper and titanium sites and their effect on the crystal structure, microstructure and dielectric properties.

Generally CCTO is made by traditional solid-state reaction from the metal oxides at high temperatures. This method needs tedious work, relatively long reaction times, and high calcination temperature. In addition some secondary phases may appear in ceramics. In contrast, synthesis from a solution leads to intimate and homogenous mixing of the metal ions at the atomic scale, thus reducing the diffusion path length required. Shorter

diffusion length leads to shorter reaction time and lower temperature. Many researchers have synthesized the undoped and doped  $\text{CaCu}_3\text{Ti}_4\text{O}_{12}$  samples at high temperature (around 1123 K for 24 h) by solid-state method.  $\text{Bi}_{2/3}\text{Cu}_3\text{Ti}_4\text{O}_{12}$  (BCTO) is isostructural with CCTO, has been reported in the literature. It indicated the temperature and frequency dependence of dielectric as CCTO.

We have synthesized the high dielectric constant materials based on Bismuth Copper Titanium by new chemical method i.e. known as semi-wet route avoiding the use of expensive titanium iso-propoxide  $\text{Ti}(\text{OR})_4$ . In this method, solutions of metal nitrates and Acetates of Bi, Cu, Zn, Mg, Ge, Ni have been used with  $\text{TiO}_2$  powder. Using this method, these materials have been synthesized at lower temperature and in short time. The mixing process is performed in a sol state. Each constituent ion is uniformly dispersed in the resulting mixture after removing organic matter by heating in air.

To the best of our knowledge, no report is available on these substituted materials synthesized by this novel route in the literature so far. The results of these investigations are reported in this thesis. There are seven chapters in this thesis.

### Chapter I

This chapter contains the introduction of the present work, describing briefly the scientific and technical investigations carried out in the field of perovskite oxides. This includes the effect of heterovalent substitutions and valency compensated substitutions on the dielectric properties. The aim of the present work is to investigate (a) crystal structure, (b) microstructure, (c) elemental analysis (d) particle size and (e) dielectric behaviour of materials prepared by semi-wet route in the following systems.

(i) BCTO  $\text{Bi}_{2/3}\text{Cu}_3\text{Ti}_4\text{O}_{12}$

(ii) BCMgTO-0.05  $\text{Bi}_{2/3}\text{Cu}_{2.95}\text{Mg}_{0.05}\text{Ti}_4\text{O}_{12}$

- (iii) BCMgTO-0.1  $\text{Bi}_{2/3}\text{Cu}_{2.9}\text{Mg}_{0.1}\text{Ti}_4\text{O}_{12}$  (iv) BCMgTO-0.2  $\text{Bi}_{2/3}\text{Cu}_{2.8}\text{Mg}_{0.2}\text{Ti}_4\text{O}_{12}$   
(v) BCNTO-0.05  $\text{Bi}_{2/3}\text{Cu}_{2.95}\text{Ni}_{0.05}\text{Ti}_4\text{O}_{12}$  (vi) BCNTO-0.1  $\text{Bi}_{2/3}\text{Cu}_{2.9}\text{Ni}_{0.1}\text{Ti}_4\text{O}_{12}$   
(vii) BCNTO-0.2  $\text{Bi}_{2/3}\text{Cu}_{2.8}\text{Ni}_{0.2}\text{Ti}_4\text{O}_{12}$  (viii) BCZTO-0.05  $\text{Bi}_{2/3}\text{Cu}_{2.95}\text{Zn}_{0.05}\text{Ti}_4\text{O}_{12}$   
(ix) BCZTO-0.1  $\text{Bi}_{2/3}\text{Cu}_{2.9}\text{Zn}_{0.1}\text{Ti}_4\text{O}_{12}$  (x) BCZTO-0.2  $\text{Bi}_{2/3}\text{Cu}_{2.8}\text{Zn}_{0.2}\text{Ti}_4\text{O}_{12}$   
(xi) BCTGO-0.05  $\text{Bi}_{2/3}\text{Cu}_3\text{Ti}_{3.95}\text{Ge}_{0.05}\text{O}_{12}$   
(xii) BCZTGO-0.05  $\text{Bi}_{2/3}\text{Cu}_{2.95}\text{Zn}_{0.05}\text{Ti}_{3.95}\text{Ge}_{0.05}\text{O}_{12}$

**Chapter II** describes the experimental techniques used for preparation and characterization of the above perovskite oxide ceramics. The semi-wet route used for preparation of these materials has been described with the help of a flow chart. Powder X-ray diffraction and scanning electron microscopy have been used for study of crystal structure and microstructure of these materials respectively. Energy Dispersive X-ray spectroscopy (EDX) technique has been used for elemental analysis of the materials. Transmission Electron Microscopy (TEM) has been used for determination of particle size in the samples. X-ray Photoelectron Spectroscopy (XPS) has been used to find the oxidation states of the elements present in the ceramics. Dielectric characteristics and Electrical Conductivity of all the samples were measured as a function of temperature (300-500 K) in the frequency range 100 Hz-10 MHz with the help of PSM 1735 Newton's 4<sup>th</sup> limited LCR Meter.

**Chapter III** contains the synthesis and characterization of the parent composition  $\text{Bi}_{2/3}\text{Cu}_3\text{Ti}_4\text{O}_{12}$  (BCTO) and Mg doped  $\text{Bi}_{2/3}\text{Cu}_{3-x}\text{Mg}_x\text{Ti}_4\text{O}_{12}$  (BCMgTO) ( $x = 0.05, 0.1$  and  $0.2$ ) compositions Pellets have been calcined at 1073 K for 6 h and sintered at 1123 K for 8 h. Single-phase formation was confirmed by XRD. Average grain size in undoped (BCTO) and Mg doped (BCMgTO) samples is  $0.70 \mu\text{m}$  and  $0.63\text{-}0.56 \mu\text{m}$  respectively

which is shown by Scanning Electron Micrographs. The stoichiometry of synthesized samples was confirmed by EDX studies. XPS spectroscopy confirmed the oxidation state of the elements present in the ceramic. On doping of  $Mg^{2+}$  concentration in CCTO, dielectric constant as well as dielectric loss of the samples decreases. Dielectric constant reduces due to decrease in concentration of oxygen vacancies which give rise to orientation polarization. A comparative dielectric study of BCTO and BCMgTO has been described in this chapter. The internal Barrier Layer Capacitance (IBLC) mechanism was responsible for the high value of the dielectric constant.

Effect of Nickel doping in  $Bi_{2/3}Cu_{3-x}Ni_xTi_4O_{12}$  ( $x = 0.05, 0.1$  and  $0.2$ ) (BCNTO) system has been described in **Chapter IV**. Compositions are synthesized by a low-temperature chemical route of the synthesis and formation of single-phase solid solution was confirmed by X-ray diffraction. Pellets were calcined at 1073 K for 6 h and sintered at 1123 K for 8 h. Scanning electron micrographs show polygonal grains morphology having grain size in the range of 0.41-0.43  $\mu m$ . Anomalous grain growth is observed in these samples. Elemental analysis is performed by EDX studies, which show the presence of Bi, Cu, Ni, Ti, and O. Particle size is determined by TEM technique. In this chapter, we have described the comparative study of structure, microstructure and dielectric properties of different doping concentration of BCNTO ceramics.

**Chapter V** contains the doping of  $Zn^{2+}$  at copper site in BCTO Ceramic. Samples of  $Bi_{2/3}Cu_{3-x}Zn_xTi_4O_{12}$  ( $x = 0, 0.05, 0.1, 0.2$ ) (BCZTO) were synthesized by semi-wet route. X-ray diffraction studies confirmed the single-phase formation at 1123 K for 8 h. Scanning electron microscopy show the grain size is in the range of 0.53-0.70  $\mu m$ . Particle size is calculated by TEM analysis. The stoichiometry of the samples is

confirmed by EDX studies. The oxidation states of the elements present in the ceramics, is confirmed by XPS. In this chapter we have also described the comparison between dielectric properties of undoped (BCTO) and doped BCZTO ceramics. The Impedance studies show the existence of Maxwell - Wagner type of relaxation phenomena in ceramics. The conductivity variation of  $\text{Bi}_{2/3}\text{Cu}_{3-x}\text{Zn}_x\text{Ti}_4\text{O}_{12}$  ceramics (where  $x= 0, 0.05, 0.1, \text{ and } 0.2$ ), with the inverse of temperature follows the Arrhenius equation, with a major temperature range of 300-500 K.

**Chapter VI** describes the effect of Ge doping at titanium site in BCTO ceramic as well as Zn and Ge simultaneous doping at copper and titanium site in BCTO ceramic respectively on the dielectric properties.  $\text{Bi}_{2/3}\text{Cu}_3\text{Ti}_{3.95}\text{Ge}_{0.05}\text{O}_{12}$  (BCTGO-0.05) and  $\text{Bi}_{2/3}\text{Cu}_{2.95}\text{Zn}_{0.05}\text{Ti}_{3.95}\text{Ge}_{0.05}\text{O}_{12}$  (BCZTGO-0.05) were synthesized by semi-wet route using  $\text{TiO}_2$  powder and metal nitrate and acetate solutions. X-ray confirmed the formation of single-phase. The microstructural analysis of the samples were done by SEM and TEM analysis. Average grain size, obtained by SEM, is 0.62  $\mu\text{m}$  and 0.68  $\mu\text{m}$  for BCTGO-0.05 and BCZTGO-0.05 respectively. Elemental analysis was performed by EDX. XPS suggests that all elements present in these ceramics are in proper oxidation states. The dielectric constant was found high for BCTGO-0.05 ceramic.

Summary and future Scope are described in **Chapter VII**.